Progress In Electromagnetics Research M, Vol. 108, 213–222, 2022

A Dual-Wideband Polarization-Insensitive Linear Polarization Converter Based on Metasurface

Jinrong Su*, Yanliang Guo, Xinwei Chen, and Wenmei Zhang

Abstract—A linear-to-linear cross-polarization converter (CPC) based on metasurface (MS) is proposed. The converter is polarization insensitive and has two wide bands. The MS is composed of periodical unit cells printed on a substrate. The top and bottom MS unit cells are formed with four groups of right-angle triangle pairs whose vertices are connected. Thus, there are eight pairs of triangles on the top and bottom surfaces of the substrate, and these pairs of triangles are arranged alternately in overlapping and orthogonal ways. The polarization conversion ratio (PCR) of the CPC is higher than 95% in the bands of 9.4 to 13.1 GHz and 13.4 to 17.2 GHz. Additionally, the PCR remains the same when the electromagnetic (EM) wave is incident at arbitrary azimuth. Furthermore, the polarization rotation angle and elliptic angle are calculated to verify the conversion effect. Finally, the conversion mechanism of the proposed converter is explored by analyzing the surface current distribution and magnetic field. The proposed converter can be applied to the field of satellite communication in Ku-band.

1. INTRODUCTION

Polarization is one of the fundamental properties of electromagnetic (EM) waves. The impact of polarization should be considered in practical applications including satellite communications, radar reception anti-interference, aerospace and medical fields [1]. Artificially controlling the polarization state of EM waves is beneficial for improving the quality of wireless communication [2]. Traditional methods to manipulate polarization are commonly accomplished by exploiting the birefringence effect of natural materials or optical crystals, which requires complex design processes and is always limited by large thickness [3]. In recent years, metasurface (MS) has opened a new approach to manipulate the polarization of EM waves. By using the extraordinary physical properties of MS, such as negative permittivity and negative permeability, the wavefront, polarization state and phase of EM wave can be manipulated artificially [4, 5]. A variety of polarization converters based on different MSs for microwave and optical bands have been proposed. They can be classified as reflection-type [6–11] and transmission-type [12–18], in which transmission-type converters are easy to assemble as they can be placed at the forward end of the radiation antenna to realize the polarization conversion of the EM wave transmitted or received. Numerous studies on transmission-type converters have been reported. For example, in [12], a transmission-type linear polarization converter has been proposed. The MS unit cell is composed of two right triangles placed diagonally and connected at the hypotenuse center. Polarization conversion ratio (PCR) of 95% can be achieved at 8.8 GHz, and the incident angle can reach 30°. In [13], four rectangles are arranged on the top surface of substrate, and other four rectangles orthogonal with the top ones are printed on the bottom of substrate, thus a MS unit cell is formed. The converter can work at the frequency range of 5.5–6.18 GHz with characteristic of polarization insensitive. In [14], a substrate integrated waveguide (SIW) based frequency selective surface is proposed to realize linear-to-linear cross-polarization conversion. The relative bandwidth is 7.2%. Also, a SIW based unit cell with

Received 29 January 2022, Accepted 23 February 2022, Scheduled 2 March 2022
* Corresponding author: Jinrong Su (sujinrong@sxu.edu.cn).
The authors are with the School of Physics and Electronic Engineering, Shanxi University, Taiyuan 030006, China.

U-shaped slots is proposed in [15], which can convert incident waves into cross-polarized waves at three frequency points with PCR close to 100%. In actual applications characteristics of wide bandwidth, polarization insensitive and larger PCR are desirable simultaneously, which needs more exploration.

In this paper, a dual-broadband, high conversion rate polarization converter with polarization insensitive is proposed. It consists of an array of four groups of right triangle pairs arranged periodically at both sides of substrate. The top and bottom triangle pairs are overlapping and orthogonal alternately. Simulated and measured results indicate that a transmission PCR of higher than 95% in the two bands of 9.4 to 13.1 GHz and 13.4 to 17.2 GHz with polarization insensitivity can be achieved. The specific design and mechanism of the MS unit cell are described in Section 2. Measured results of the proposed polarization converter are given in Section 3, and the conclusion is drawn in Section 4.

2. DESIGN AND PRINCIPLES

2.1. Metasurface Unit Cell Structure

It is well known that in the design of CPC, orthogonal patches on the top and bottom surfaces produce orthogonal electric fields, while parallel ones can form Fabry-Perot (FP) resonator-like cavities [18]. Both can convert linearly polarized incident waves into cross-polarized ones. In this paper, the above two principles are combined to construct the CPC MS unit cell.

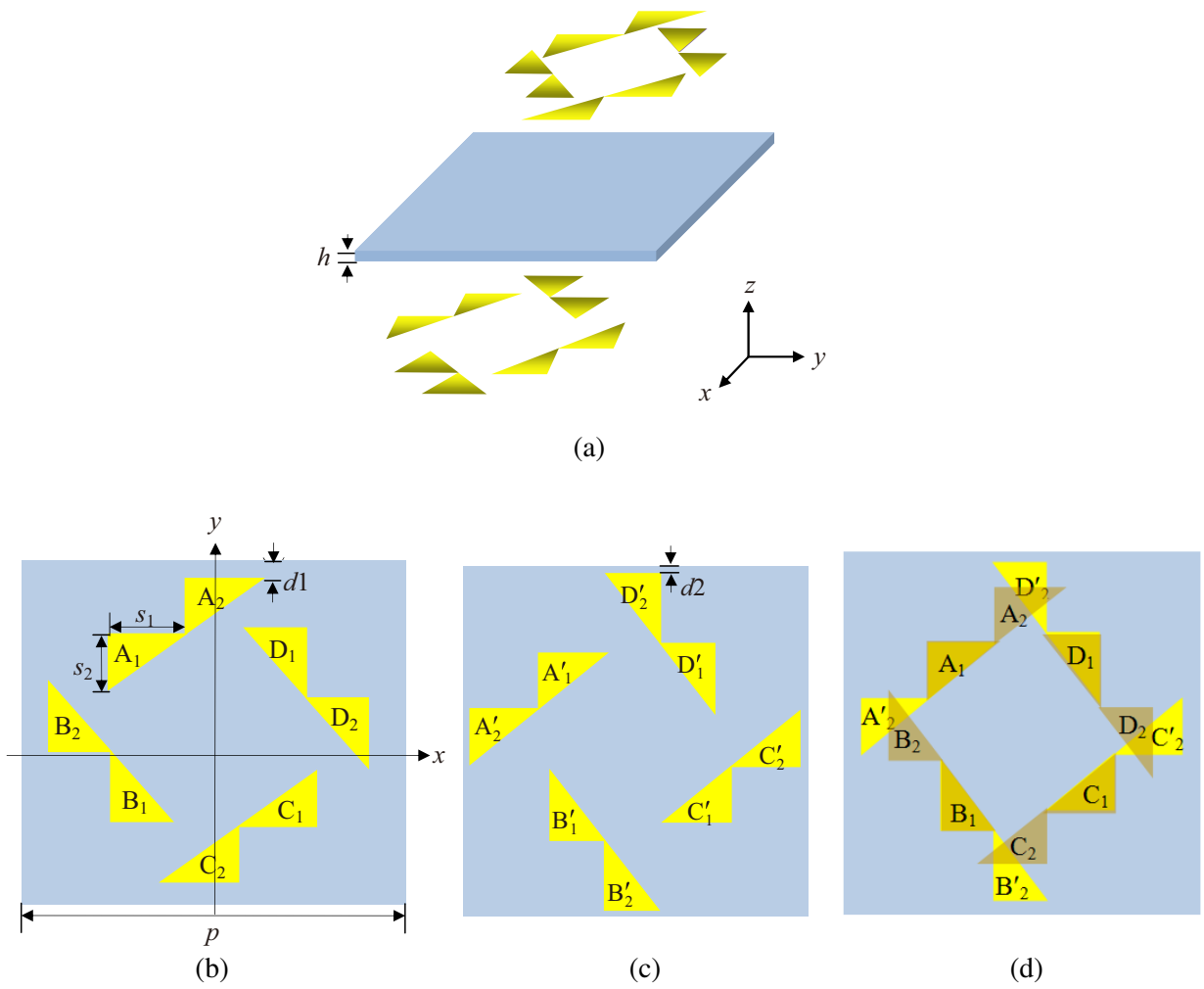

Figure 1. Scheme of the proposed MS unit cell: (a) Unit cell structure, (b) top view, (c) bottom view and (d) perspective view from the top.

The CPC MS unit cell is formed by a substrate and periodically repeating triangular pairs of copper patches. The structure of unit cell is illustrated in Figure 1(a). The dielectric substrate is Rogers 4725 with a loss angle tangent of 0.0022 and relative permittivity of 2.55, and the size is $23 \times 23 \times 0.762\,\text{mm}^3$. There are four steps to form the unit cell. Firstly, two right triangles are placed collinear with hypotenuse, and the vertices are connected to form a triangular pair named A. Secondly, pair A is rotated counterclockwise around the center of the dielectric substrate by 90°, 180°, and 270° to obtain triangular pairs B, C, and D. The four pairs form the top MS unit cell, as plotted in Figure 1(b). Thirdly, pair A is translated along the negative direction of x, y, and z axes by s_1, s_2, and h, respectively, to form a triangle pair A′. Note that pair A′ is on the bottom of the substrate. Fourthly, pair A′ is rotated around the center of the substrate counterclockwise by 90°, 180°, and 270° to form triangle pairs B′, C′, and D′, which together with pair A′ form the bottom MS unit cell, as shown in Figure 1(c). In each pair of triangles, the one overlaps the bottom (top) one is marked 1, and the other one orthogonal to the bottom (top) one is marked 2, as shown in Figure 1(d). For example, in pair A, A_1 overlaps A_1', and A_2 is orthogonal to D_2'. The optimized geometric parameters are shown in Table 1.

Table 1. Optimized parameters of the CPC.

parameters	size/mm
p	23
d	6
d_1	1.5
d_2	0.5
s_1	5
s_2	4
h	0.762

2.2. Performance and Analysis

2.2.1. Polarization Conversion Performance Analysis

Finite-Difference Time-Domain (FDTD) method based software CST Microwave Studio is used to simulate and analyze the structure. Figure 2 shows the amplitudes of transmitted wave for y-polarized normal incident wave, where T_{yy} and T_{xy} are the co- and cross-polarization transmission coefficients, respectively. x and y denote the polarization direction of the incident wave. One can see that the amplitude of T_{xy} is above -3 dB in the two bands of 9.4 to 13.1 GHz and 13.4 to 17.2 GHz, while the amplitude of T_{yy} is less than -15 dB, indicating that cross-polarization conversion of incident waves is achieved.

Besides, the phase difference δ between co- and cross-polarization transmitted waves is plotted in blue in Figure 2. One can see that δ is 180° at frequencies from 9.4–13.1 GHz and 15.7–17.2 GHz, and 360° at frequencies from 13.4–15.7 GHz. Here, δ is used to calculate the polarization rotation angle α and ellipticity angle β to further verify the polarization conversion state. Firstly, Stokes parameters are calculated as follows [19]:

$$S_0 = T_{yy}^2 + T_{xy}^2 \tag{1}$$

$$S_1 = T_{yy}^2 - T_{xy}^2 \tag{2}$$

$$S_2 = 2T_{yy}T_{xy}\cos\delta \tag{3}$$

$$S_3 = 2T_{yy}T_{xy}\sin\delta \tag{4}$$

Then, the polarization rotation angle α and the elliptic angle β can be calculated by

$$\alpha = \frac{1}{2}\tan^{-1}\left(\frac{S_2}{S_1}\right) \tag{5}$$

$$\beta = \frac{1}{2}\tan^{-1}\left(\frac{S_3}{S_0}\right) \tag{6}$$

Note that if α is 90°, the polarization conversion is achieved, and it is purely linear polarization if β is 0°. The calculated α and β are plotted in Figure 3. One can see that α is 90°, and β is 0° at frequency ranges of 9.4 to 13.1 GHz and 13.4 to 17.2 GHz, implying that the designed CPC can achieve a near-perfectly linear cross-polarization conversion.

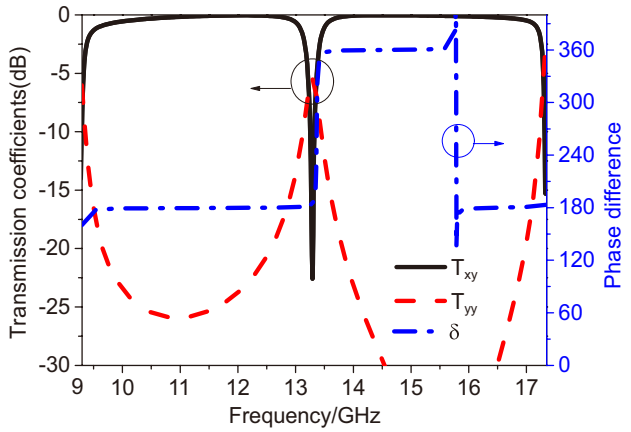

Figure 2. Co- and cross-polarization transmission coefficients of the unit cell in the operating frequency bands.

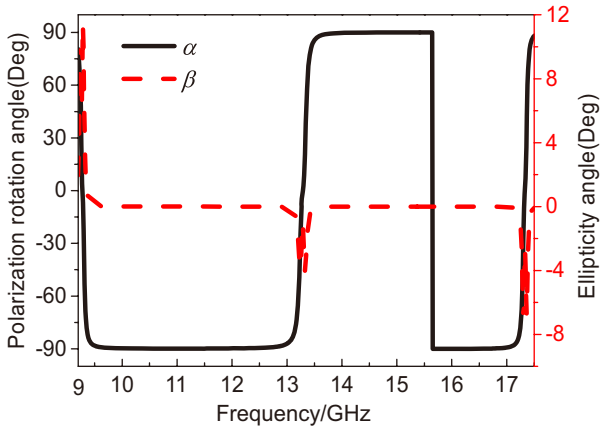

Figure 3. Polarization rotation angle α and elliptic angle β in the operating frequency bands.

In addition, PCR is generally used to describe the polarization conversion efficiency, which can be calculated by [15]

$$\mathrm{PCR} = \frac{T_{xy}^2}{T_{xy}^2 + T_{yy}^2 + R_{xy}^2 + R_{yy}^2} \tag{7}$$

Here R_{yy} and R_{xy} are the magnitudes of the co- and cross-polarization reflection coefficients. Figure 4 illustrates the PCR of the converter for y-polarized normal incident wave. One can see that PCR is higher than 95% in both frequency ranges of 9.4 to 13.1 GHz and 13.4 to 17.2 GHz. The high PCR is mainly due to low loss material and ingenious design. Ultra-thin Rogers 4725 substrate with 0.762 mm thickness is beneficial for reducing the loss of wave transmission. The insertion loss (IT) can be calculated

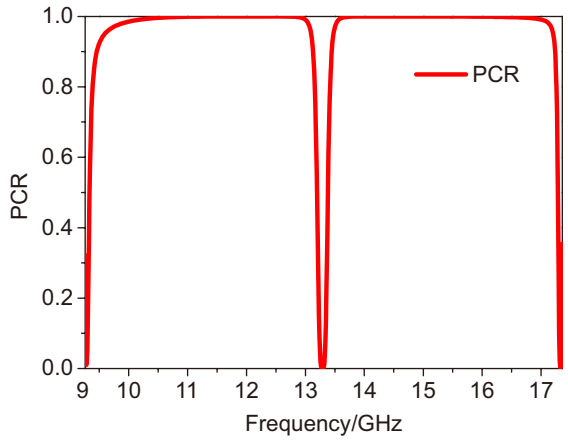

Figure 4. PCR of the unit cell in the operating bands.

by [20]

$$\mathrm{IT} = 1 - |T_{xy}|^2 - |T_{yy}|^2 - |R_{xy}|^2 - |R_{yy}|^2 \tag{8}$$

and it is smaller than 0.005 over the operating bands. The extremely low insertion loss ensures that most of incident wave energy can be transmitted, resulting in a high PCR. Besides, the ingenious arrangement of triangle pairs allows each triangle to participate in the polarization conversion, as explained in the following Subsection 2.2.2, which produces high PCR.

2.2.2. Analysis of Polarization Conversion Principles

To explain the polarization conversion principles, Figure 5 shows the surface current distributed at the top and bottom surfaces of the unit cell at 12 GHz. The incident wave is also normal incident y-polarized wave. In Figures 5(a) and (b), the surface currents of the four pairs of triangles A_1-A'_1, B_1-B'_1, C_1-C'_1, and D_1-D'_1 with overlapping positions flow in opposite directions and mainly along the hypotenuse. The hypotenuse currents of A_1 and C_1 are in the same direction, and they are noted as $\mathbf{J_1}$. Those of A'_1 and C'_1 are noted as $\mathbf{J'_1}$. Similarly, the hypotenuse currents of B_1 and D_1, B'_1 and D'_1 are noted as $\mathbf{J_2}$ and $\mathbf{J'_2}$, respectively. $\mathbf{J_1}$ and $\mathbf{J'_1}$ will excite the magnetic field $\mathbf{H_1}$, while $\mathbf{J_2}$ and $\mathbf{J'_2}$ will excite the magnetic field $\mathbf{H_2}$, as shown in Figure 5(c). $\mathbf{H_1}$ can be decomposed into $\mathbf{H_{1x}}$ along x-axis and $\mathbf{H_{1y}}$ along the negative y-axis. Also, $\mathbf{H_2}$ is resolved into $\mathbf{H_{2x}}$ along the negative x-axis and $\mathbf{H_{2y}}$ along the negative y-axis. According to the Maxwell's Equations, $\mathbf{H_{1y}}$ and $\mathbf{H_{2y}}$ produce x-polarized electric field. Additionally, for the orthogonal triangle pairs A_2-D'_2, B_2-A'_2, C_2-B'_2, and D_2-C'_2, the surface currents at top triangles and that coupled to the bottom ones are orthogonal, which induce electric field orthogonal to that of incident wave. Thus, the polarization of incident wave is converted into cross polarization.

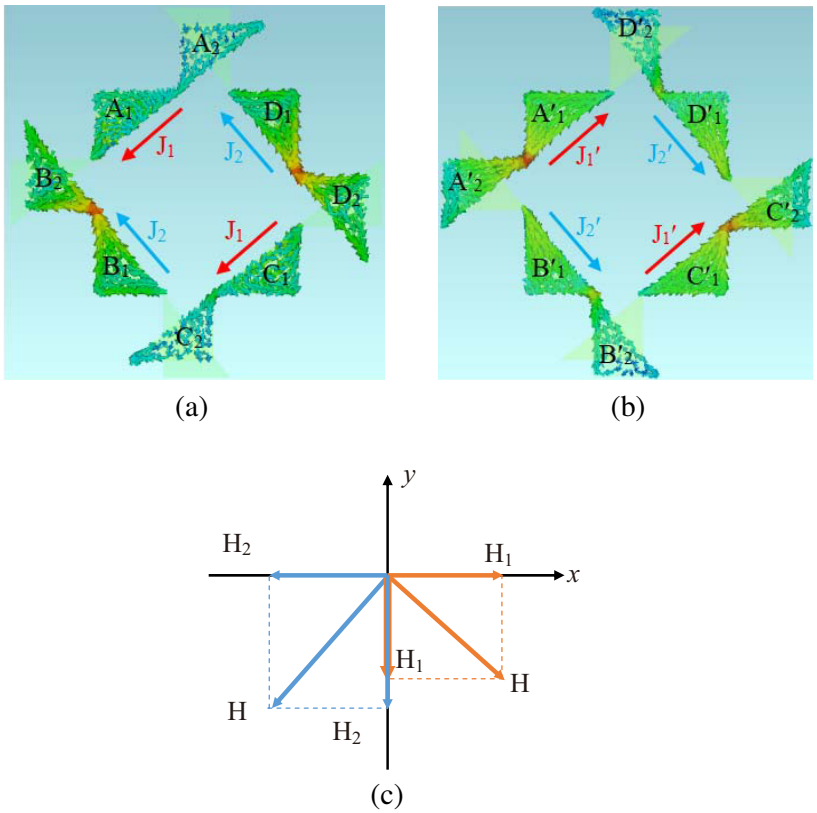

Figure 5. Surface current distributed at the top and bottom of the unit cell at 12 GHz: (a) Top surface (b) bottom surface and (c) magnetic field decomposition diagram.

2.2.3. Polarization Insensitivity

To fully explore the conversion performance, PCR is simulated when the incident azimuth φ_i varies from 0° to 90°. The polarization azimuth angle φ_i is the angle between the electric field direction of incident wave (v-axis in Figure 6) and y-axis, as shown in Figure 6. For example, when the electric field is along y-axis (y-polarization), φ_i is 0°. Figure 7 plots PCR for normal incident wave with different φ_i. One can see that PCR remains the same when φ_i varies from 0° to 90°, indicating that the designed polarization converter is polarization insensitive. The reason for this is the arrangement of the triangle pairs. Pairs A (or C) and B (or D) can convert incident waves with azimuth of 0° and 90°, respectively. Waves incident at any azimuth can be resolved into waves of 0° and 90°, and then they are converted into cross-polarization.

In addition, to better verify the polarization insensitive characteristic, Figure 8 shows the electric field of normal incident wave with φ_i of 0°, 30°, 60°, and 90° at 12 GHz. When φ_i is 0°, the transmitted wave is perpendicular to the incident wave, i.e., a 90° cross-polarization conversion is achieved. Also, when φ_i is 30°, 60°, and 90°, respectively, 90° rotations are achieved in the transmitted waves.

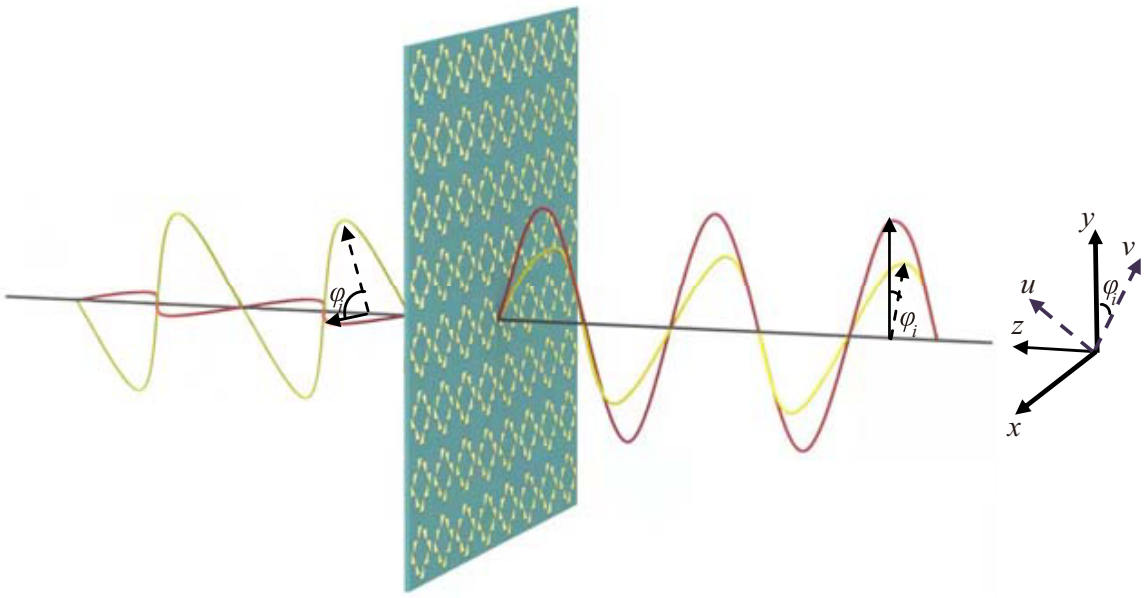

Figure 6. Polarization azimuth angle φ_i.

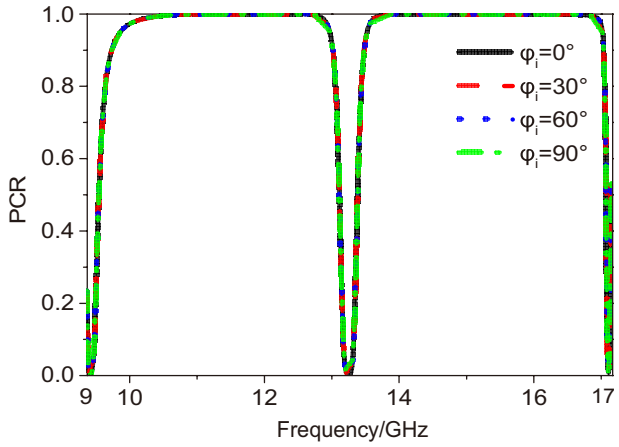

Figure 7. PCR of the converter when azimuth of incident wave varying from 0° to 90°.

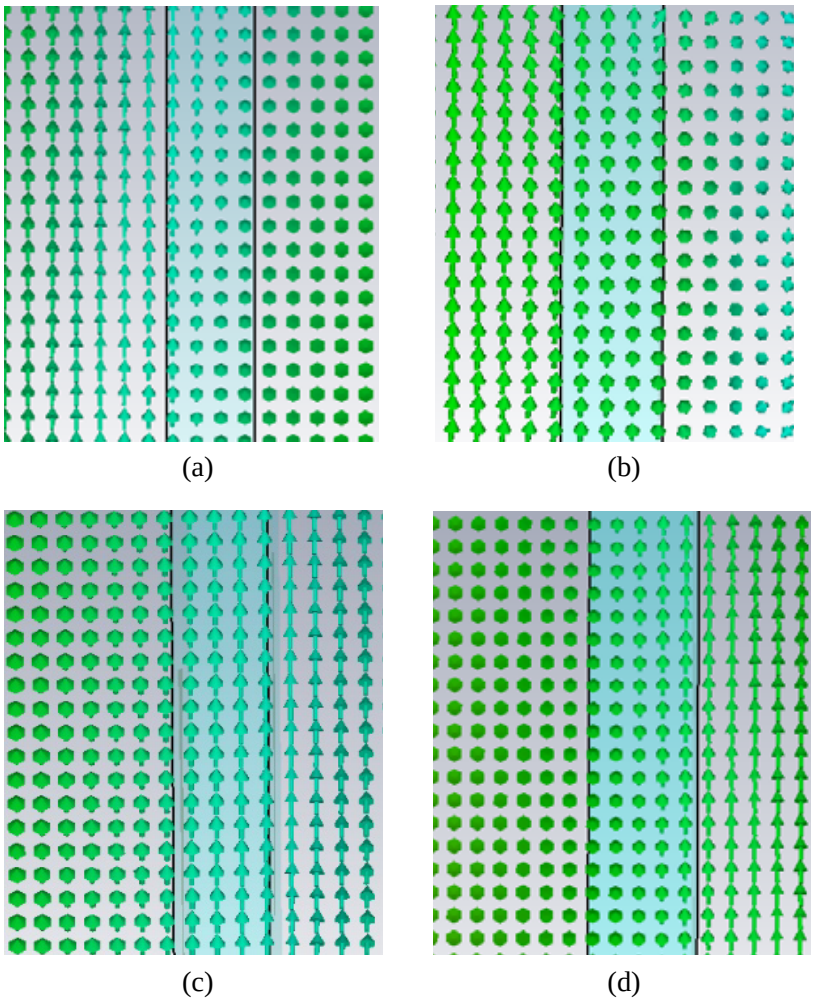

Figure 8. Simulated electrical field distributions for normal incident wave with (a) $\varphi_i = 0°$, (b) $\varphi_i = 30°$, (c) $\varphi_i = 60°$ and (d) $\varphi_i = 90°$.

3. RESULTS AND DISCUSSION

For the purpose of verifying the feasibility of the design, a prototype of the designed CPC consisting of 8×8 MS unit cells is fabricated. Photographs of the top and bottom surfaces are shown in Figure 9. The unit cell geometries are the same as that of simulation, and the overall size of the sample is $184 \times 184\,\text{mm}^2$.

The measurement environment is shown in Figure 10. The sample is surrounded by absorbent material, and two standard horn antennas, LB-20180-SF with operating band of 2–18 GHz and aperture D of 130 mm, are placed at the two ends of the sample. The center of the sample is collinear with the center of the two horn antennas, and the distance d between the transmitting horn antenna and the sample is larger than the far field of the antenna $2D^2/\lambda$. The horn antennas are connected to the network vector analyzer N5222A to measure the transmission coefficient. Both horn antennas are placed horizontally to obtain T_{yy}, and T_{xy} is obtained by rotating the receiving antenna by 90°.

Figure 11 depicts the simulated and measured T_{xy} varying with frequency. It indicates that the measured results are basically consistent with the simulated ones. The reason for the error is mainly the limited number of unit cell repetitions of the sample.

Table 2 compares different transmission-type linear-to-linear CPCs. One can see that the proposed

Figure 9. Photographs of the sample: (a) Top view and (b) bottom view.

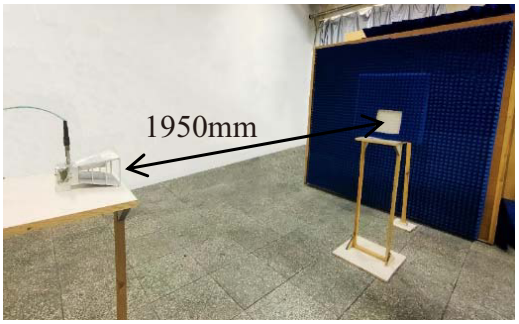

Figure 10. Measuring environment.

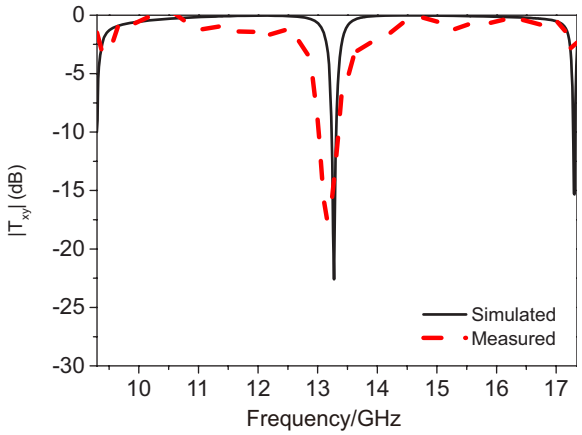

Figure 11. Simulated and measured results.

converter has large relative bandwidth and small thickness. Additionally, the PCR of this converter is higher than 95%, and it is polarization insensitive. Thus, the converter in this work has excellent conversion performance.

Table 2. Comparisons between the proposed converter and other works.

Refs.	Unit cell size (mm^3)	Operating frequency (GHz)	Relative bandwidth	PCR	Polarization insensitive
[12]	$8 \times 8 \times 0.8$	8.8	-	95%	$T_{yx} = T_{xy}$
[13]	$18 \times 18 \times 2$	5.8–6.18	6.3%	$> 80\%$	0–45°
[14]	$6 \times 6 \times 1.57$	34.16–36.7	7.2%	$> 80\%$	$T_{yx} = T_{xy}$
[15]	$16 \times 16 \times 3.175$	6.82&9.4&12.02	-	100%	no
[18]	$14 \times 14 \times 0.762$	11.4	-	$> 90\%$	0–90°
This work	$23 \times 23 \times 0.762$	9.4–13.1	32.9%	$> 95\%$	0–90°
		13.4–17.2	24.8%		

4. CONCLUSIONS

A transmission type linear-to-linear CPC based on metasurface is proposed. Four groups of triangle pairs are arranged at top and bottom sides of the substrate, and the eight pairs of triangles on both sides are arranged alternately in overlapping and orthogonal ways. More than 95% PCR has been achieved in frequency ranges of 9.4 to 13.1 GHz (32.9%) and 13.4 to 17.2 GHz (24.8%) with characteristic of polarization insensitivity. The polarization converter is simple in structure, thin in thickness, and easy to integrate. It is a good candidate for Ku-band wireless communications such as satellite communications.

ACKNOWLEDGMENT

This work was supported by the National Natural Science Foundation of China (No. 62071282).

REFERENCES

1. Zhao, Y. and A. Alù, "Manipulating light polarization with ultrathin plasmonic metasurfaces," *Phys. Rev. B: Condens. Matter*, Vol. 84, No. 20, 205–428, 2011.
2. Sun, W. J., Q. He, J. M. Hao, and L. Zhou, "A transparent metamaterial to manipulate electromagnetic wave polarization," *Optics Letters*, Vol. 36, No. 6, 927–929, 2011.
3. Peng, L., X. F. Li, X. Jiang, and S. M. Li, "A novel THz half-wave polarization converter for cross-polarization conversions of both linear and circular polarizations and polarization conversion ratio regulating," *Journal of Lightwave Technology*, Vol. 36, No. 19, 4250–4258, 2018.
4. Shelby, R. A., D. R. Smith, and S. Schultz, "Experimental verification of a negative index of refraction," *Science*, Vol. 292, No. 5514, 77–79, 2001.
5. Zhu, W. R., X. P. Zhao, and J. Q. Guo, "Multibands of negative refractive indexes in the left-handed metamaterials with multiple dendritic structures," *Applied Physics Letters*, Vol. 92, No. 24, 241116, 2008.
6. Gao, X., X. Han, W. P. Cao, H. O. Li, H. F. Ma, and T. J. Cui, "Ultrawideband and high-efficiency linear polarization converter based on double V-shaped metasurface," *IEEE Transactions on Antennas and Propagation*, Vol. 63, No. 8, 3522–3530, 2015.
7. Chakravarty, S. and D. Mitra, "A novel ultra-wideband and multifunctional reflective polarization converter," *2020 IEEE 17th India Council International Conference (INDICON)*, 1–4, 2020.
8. Kamal, B., J. Chen, Y. Yin, J. Ren, S. Ullah, and U. Ali, "Design and experimental analysis of dual-band polarization converting metasurface," *IEEE Antennas and Wireless Propagation Letters*, Vol. 20, No. 8, 1409–1413, 2021.
9. Yu, H. and J. Su, "Dual-band and high-efficiency reflective polarization converter based on strip grating," *2020 IEEE International Symposium on Antennas and Propagation and North American Radio Science Meeting*, 967–968, 2020.
10. Zhou, Q., G. Du, and D. Wang, "Ultra-broadband linear polarization converter based on single-layer reflective metasurface," *2020 IEEE MTT-S International Conference on Numerical Electromagnetic and Multiphysics Modeling and Optimization (NEMO)*, 1–4, 2020.
11. Karamirad, M., C. Ghobadi, and J. Nourinia, "Metasurfaces for wideband and efficient polarization rotation," *IEEE Transactions on Antennas and Propagation*, Vol. 69, No. 3, 1799–1804, 2021.
12. Baghel, A. K., S. S. Kulkarni, and S. K. Nayak, "Linear-to-cross-polarization transmission converter using ultrathin and smaller periodicity metasurface," *IEEE Antennas and Wireless Propagation Letters*, Vol. 18, No. 7, 1433–1437, 2019.
13. Wang, S. Y., J. D. Bi, W. Liu, W. Geyi, and S. Gao, "Polarization-insensitive cross-polarization converter," *IEEE Transactions on Antennas and Propagation*, Vol. 69, No. 8, 4670–4680, 2021.
14. Zhu, X., et al., "Design of a bandwidth-enhanced polarization rotating frequency selective surface," *IEEE Transactions on Antennas and Propagation*, Vol. 62, No. 2, 940–944, 2014.

15. Du, X., H. Lin, X. Shi, Y. Mao, and Y. Wu, "Triple-band metamaterial polarization converter based on substrate integrated waveguide technology," *2020 Cross Strait Radio Science & Wireless Technology Conference (CSRSWTC)*, 1–3, 2020.
16. Ye, Y. Q. and S. L. He, "90° polarization rotator using a bilayered chiral metamaterial with giant optical activity," *Applied Physics Letters*, Vol. 96, 203501, 2010.
17. Nandi, R., Nilotpal, and S. Bhattacharyya, "A transmittive type broadband cross polarization converter for mid wavelength infrared region," *2019 URSI Asia-Pacific Radio Science Conference (AP-RASC)*, 1–4, 2019.
18. Song, K., Y. H. Liu, Q. H. Fu, X. P. Zhao, C. R. Luo, and W. R. Zhu, "90° polarization rotator with rotation angle independent of substrate permittivity and incident angles using a composite chiral metamaterial," *Opt. Express*, Vol. 21, No. 6, 7439–7446, 2013.
19. Jing, X., X. Gui, P. Zhou, and Z. Hong, "Physical explanation of Fabry-Pérot cavity for broadband bilayer metamaterials polarization converter," *Journal of Lightwave Technology*, Vol. 36, No. 12, 2322–2327, 2018.
20. Liu, W., "Design of polarization converters based on frequency selective surface," Master's Thesis, Nanjing University of Information Science & Technology, 2018.